Electron-Beam Guiding and Phase-Mix Damping by an Electrostatically Charged Wire

D. S. Prono, G. J. Caporaso, A. G. Cole, R. J. Briggs, Y. P. Chong, J. C. Clark, R. E. Hester, E. J. Lauer, R. L. Spoerlein, and K. W. Struve

University of California, Lawrence Livermore National Laboratory, Livermore, California 94550

(Received 4 April 1983)

A new and relatively simple method has been developed to focus and guide electron beams without the use of a magnetic field. The scheme relies on the electrostatic charging of a highly resistive wire in the presence of a beam. The beam is then strongly guided and focused by the oppositely charged wire. In addition, the highly anharmonic nature of the wire potential leads to rapid phase-mix damping of transverse beam displacements and radial pulsations.

PACS numbers: 07.77.+p, 41.80.Dd

Accelerators that produce high current and high particle-energy electron beams are often plagued with difficulties in beam guidance, and, more importantly, in damping out unwanted beam motion. For example, in linear induction accelerators where numerous accelerating cavities are used, a cavity-mode–beam interaction, the beam-breakup instability (BBU),[1] impresses transverse oscillations on the beam. For many applications, transverse motion of the beam is an undesirable phenomenon that adversely affects beam propagation. In this paper we summarize analytic models and simulations (Caporaso and Cole[2]) and experimental results with a simple electrostatic-focusing technique of Prono *et al.* that phase mixes (damps) coherent, transverse beam motion into increased beam emittance.[3]

Consider a highly resistive wire placed along the axis of a conducting pipe and supported by electrically conducting end foils. When an electron beam is injected into such a configuration, the wire becomes positively charged to the degree necessary to maintain its surface at the same potential as that of the pipe. The transient currents needed for this charge redistribution die out quickly because of the small L/R (~2 ns) time constant of the system. The pipe, wire, and beam radii and profile are then sufficient to determine the linear charge density on the wire. For example, for a parabolic beam with current density proportional to $1-r^2/a^2$, one finds from setting the integral of the radial electric field from a_w to b equal to zero that

$$f=-\frac{\lambda_{\text{wire}}}{\lambda_{\text{beam}}}=\frac{\frac{3}{4}+\frac{1}{4}(a_w/a)^4-(a_w/a)^2+\ln(b/a)}{\ln(b/a_w)}, \tag{1}$$

where a_w, a, and b are the wire, beam edge, and pipe radii, respectively. For typical parameters of interest $f\cong 0.5$. The wire is thus very strongly charged.

For relativistic electrons, the dominant force is due to the wire since the space-charge repulsion and self-pinch forces on the beam cancel to $O(1/\gamma^2)$. Thus in the *paraxial approximation*,[4] the equation of motion for a beam electron is

$$\gamma m v^2\,\partial^2\vec{r}/\partial z^2=-(2efI_b/vr^2)\vec{r}. \tag{2}$$

Here fI_b/v is the wire-charge density (I_b is the beam current, v the axial velocity of the electrons), $\gamma=(1-v^2/c^2)^{-1/2}$, m and e are the electron rest mass and charge, respectively, $\vec{r}$ is the radius vector from the wire center to the electron in a plane transverse to the wire axis, and z is distance along the axis. We developed a particle code to solve an extended version of Eq. (2) that includes the effects of focusing magnets.

The potential corresponding to the force in Eq. (2) is proportional to $\ln(r)$. Beam particles orbiting in an anharmonic potential give rise to a dissipationless process known as phase-mix damping.[5] That is, any coherent motion of the beam will eventually damp out since the orbital frequencies of the particles depend on their transverse energies and angular momenta. As this damping occurs, the emittance or area occupied by the beam in its transverse phase space increases. Taking the dot product of Eq. (2) with $\vec{r}$, averaging the result over the beam profile, and applying the definition of emittance for a beam with no net canonical or mechanical angular momentum,[6] we obtain an envelope equation for the root-mean-square (rms) radius of the beam in the presence of the wire field,

$$\partial^2R/\partial z^2=E^2/R^3-2fI_b/\beta^2I_AR, \tag{3}$$

where $I_A=\gamma\beta mc^3/e=17\,000\beta\gamma$ A, R and E are the

rms radius and emittance, respectively, and $\beta = v/c$. Setting $\partial^2 R/\partial z^2 = 0$ gives the equilibrium or matched radius for injection onto the wire, $R_m = E(\beta^2 I_A/2fI_b)^{1/2}$. Injection of a beam onto a wire at other than the matched radius will lead to radial pulsations that will result in phase-mix damping with an attendant emittance rise. Injection of a beam transversely displaced from the wire axis will also lead to an emittance increase as the beam offset undergoes phase-mix damping.

Results shown in Fig. 1 are for a simulation that corresponds to these processes. Figure 1(a) shows the axial magnetic field provided by the focusing elements; Figs. 1(b) and 1(c), the resulting rms radius and emittance, respectively; and Fig. 1(d), the radial position of the beam centroid. The beam is injected onto the wire with a radius that is too large (for the conditions of Fig. 1, $R_m \sim 3$ mm). In addition, the beam is injected into the transport section so that its centroid is offset as it enters the wire field. The damping of the pulsations and transverse offset and the consequent increase in emittance are clearly evident.

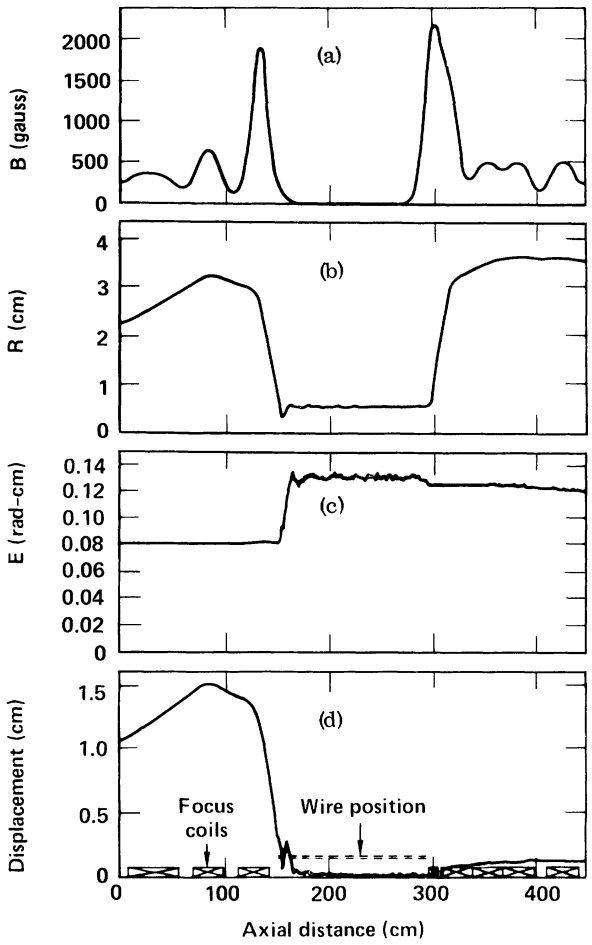

FIG. 1. Simulation results for beam propagation on a wire, with configuration shown in Fig. 3: (a) Axial magnetic field provided by focusing elements; (b), (c) resulting rms radius and emittance, respectively; and (d) radial position of the centroid. At bottom of figure, the dotted line between 150 and 300 cm indicates position of the wire and the boxes indicate locations of focus coils shown in Fig. 3.

One interesting and important consequence of beam propagation on a wire can be deduced from Eq. (2). If $\vec{r}$ is dotted into Eq. (2), the result is summed over all particles, and the customary definitions of rms perpendicular velocity and beam radius are used, we obtain

$$\frac{1}{2}\left(\frac{\partial^2 R^2}{\partial z^2}\right) - \left(\frac{v_\perp^2}{v^2}\right) = \frac{-2fI_b}{\beta^2 I_A} . \quad (4)$$

In equilibrium we have $v_\perp/c = (2fI_b/I_A)^{1/2}$. For the conditions in Fig. 1, $v_\perp/c \cong 0.2$ at the end of the wire. Thus large magnetic fields are required to control the beam expansion as it exists from the wire [see curve (a) of Fig. 1].

Results from two experimental configurations (Figs. 2 and 3) are now presented. In configuration I we tested survivability of the graphite wire and tested the focusing/guiding effects of the system. This configuration (Fig. 2) consisted of a 1-m-long, 15-cm-diam, experimental tank connected to the experimental test accelerator (ETA) vacuum beam line and evacuated to $<10^{-5}$ Torr. The entrance to the tank was a 6-cm-diam aperture covered by a 0.001-in.-thick titanium foil. The wire passed through a small (1-mm-diam) supporting graphite cradle at the center of the entrance foil. This end of the wire was firmly anchored to the outer periphery of the foil; the other end was kept in tension by passing it through a second foil and then attaching it to a weight. The wire is $\lesssim 1$ mm in diameter and consists of many twisted, long, graphite fibers, with a line resistance of $\sim 1000\ \Omega/m$. Such a configuration survives several days without failure (the accelerator is the ETA,[7] which produces a beam of 8 kA, 30 ns, 4.5 MeV, 0.75-cm radius, with beam emittance $\cong 0.08$ rad cm, and with a 1-s^{-1} pulse rate that continuously operates for up to 8 h/d). Note that the wire was drawn through a second 6-cm-diam aperture (without foil) located 80 cm downstream; this tested the focusing capability of the system. Diagnostic devices, monitoring the time variation of beam current and displace-

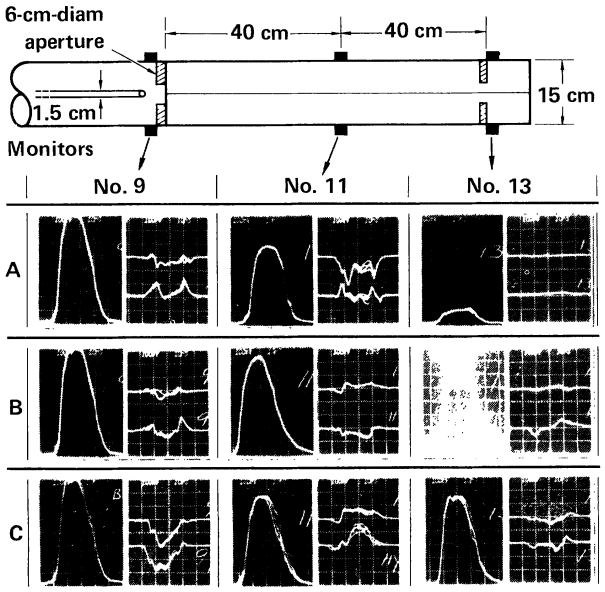

FIG. 2. Tests with configuration I. The schematic indicates the experimental arrangement. Shown are measurements of current and centroid displacement at three axial locations (0, 40, or 80 cm) for the test cases A, B, and C described in the text. For each monitor, left trace is beam current (1 kA/div, 10 ns/div); right trace is current-weighted, beam-centroid displacement from axis in X plane (top), and Y plane (bottom) at peak current ($\frac{1}{2}$ cm/div, 10 ns/div).

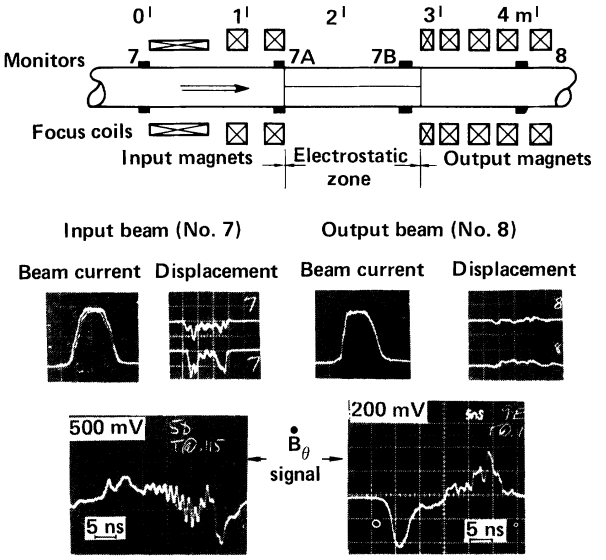

FIG. 3. Test with configuration II. The schematic indicates the experimental arrangement. The beam current (2 kA/div, 10 ns/div) and current-weighted, beam-centroid displacement (at peak current 1 cm/div, 10 ns/div) are recorded from monitors before and after the wire zone. The $\dot{B}_\theta$ signals, taken before and after the electrostatic zone, are proportional to $d/dt(I_B/r)$, where r is distance from beam to probe. Four probes, each 90° apart, were actually used at each axial location to account for geometric correction factors. The downstream $\dot{B}_\theta$ scale is 2.5 times more sensitive than the upstream.

ment of the beam centroid in two orthogonal planes, were located immediately preceding the entrance foil to the tank and also at 40 and 80 cm, immediately after the last aperture.[8] A TV screen was also used to view beam-induced light from the entrance foil and to estimate beam radius on injection.

Results of three test cases run with configuration I are shown in Fig. 2. These tests were (A) beam transport with beam injected on axis but no electrostatic focusing, (B) beam transport with the electrostatic wire installed and beam injected on axis, and (C) beam transport with electrostatic wire and with the beam injected 1.5 cm off axis. Case A shows a decrease in transported current that is consistent with emittance-dominated beam expansion. The results of tests B and C demonstrate the focusing, guiding, and centering capabilities of the electrostatic wire.

The experimental arrangement for configuration II is schematically shown in Fig. 3 (top); this was the setup modeled by the simulation of Fig. 1. Here the electrostatic wire zone is located within a beam-transport system. This allowed study of the dynamics of matching a beam into the zone and then transporting the beam after it left the zone.

Diagnostics consisted of current monitors before and after the zone (total current and centroid movement), a TV to determine entrance-beam size, and pairs of $\dot{B}_\theta$ probes (before and after the zone), which sense the magnitude of the BBU high-frequency (800 MHz) spatial oscillations. The supporting foils are 0.003-in-thick graphite and are separated by 1.4 m. For the experimental results shown, the aperture of the exit foil was a 4-cm-diam, thick, graphite annulus.

The initial portion of the current pulse is not strongly focused by the wire because the beam current is low and transient currents have not yet died out. This results in current loss to the walls, which causes a sharpening of the beam rise time. As the data show, an input beam monitored upstream from the matching-focus magnets of the wire zone has an approximate 8-

ns rise time and has significant spatial oscillations of the beam centroid (especially of the beam head and tail). The current monitor located downstream of the wire zone and halfway through the output matching-focus magnets measures 90% current transmission with a rise time sharpened to ~3 ns with the amplitude of the centroid displacement decreased by factors of 5 to 10. The oscilloscope traces of the $\dot{B}_\theta$ probes located before and after the wire zone show the sharpened rise time and the decreased (by a factor of 5 to 10) 800-MHz BBU oscillations. Additional diagnostics indicate that beam emittance approximately doubles when the wire zone is in place. This emittance increase, attributed to phase-mix damping of transverse motion and to mismatched injection, is consistent with the simulation predictions shown in Fig. 1.

In summary, a new and simple method for beam transport and control is described. Experimental results are in qualitative agreement with simulations that show effective focusing and damping of a transversely displaced electron beam. The technique promises to be of significant benefit in reducing the amplitudes of various accelerator-related instabilities and undesirable transverse-beam offsets.

The technical support of the ETA operations staff is gratefully acknowledged, with special thanks to R. Hill. This work was performed jointly under the auspices of the U. S. Department of Energy by the Lawrence Livermore National Laboratory under Contract No. W-7405-ENG-48 and of the U. S. Department of Defense under Defense Advanced Research Projects Agency ARPA Order No. 4395 A No. 12, monitored by the U. S. Naval Surface Weapons Center under Document No. N60921-83-WR-W0113.

[1]V. K. Neil, L. S Hall, and R. K. Cooper, Part. Accel. 9, 213 (1979).

[2]G. J. Caporaso and A. G. Cole, IEEE Trans. Nucl. Sci. 30, 2618 (1983).

[3]D. S. Prono *et al.*, IEEE Trans. Nucl. Sci. 30, 2510 (1983).

[4]E. P. Lee, Phys. Fluids 19, 60 (1976).

[5]E. P. Lee, Phys. Fluids 21, 1327 (1978).

[6]E. P. Lee and R. K. Cooper, Part. Accel. 7, 83 (1976).

[7]T. J. Fessenden *et al.*, in Proceedings of the Fourth International Topical Conference on High-Power Electron and Ion-Beam Research and Technology, Palaiseau, France, 1981 (unpublished), p. 813.

[8]T. J. Fessenden, B. W. Stallard, and G. G. Berg, Rev. Sci. Instrum. 43, 1789 (1972).

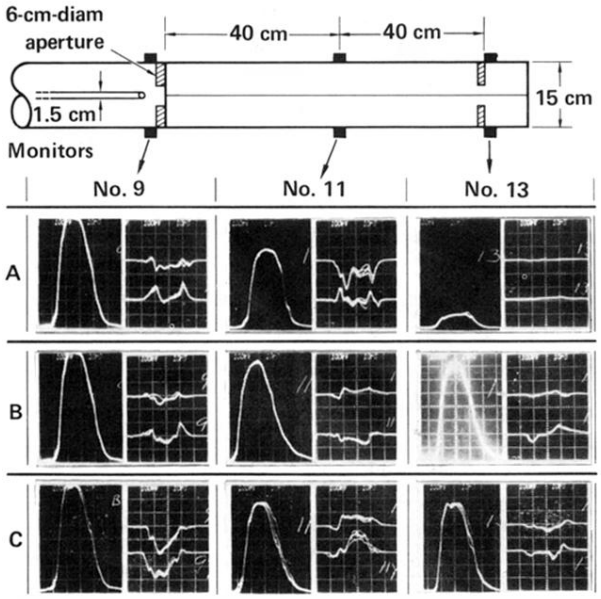

FIG. 2. Tests with configuration I. The schematic indicates the experimental arrangement. Shown are measurements of current and centroid displacement at three axial locations (0, 40, or 80 cm) for the test cases A, B, and C described in the text. For each monitor, left trace is beam current (1 kA/div, 10 ns/div); right trace is current-weighted, beam-centroid displacement from axis in X plane (top), and Y plane (bottom) at peak current ($\frac{1}{2}$ cm/div, 10 ns/div).

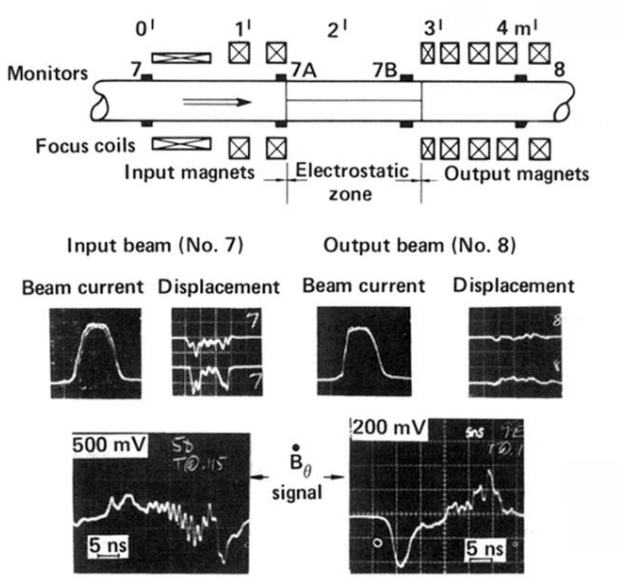

FIG. 3. Test with configuration II. The schematic indicates the experimental arrangement. The beam current (2 kA/div, 10 ns/div) and current-weighted, beam-centroid displacement (at peak current 1 cm/div, 10 ns/div) are recorded from monitors before and after the wire zone. The $\dot{B}_\theta$ signals, taken before and after the electrostatic zone, are proportional to $d/dt(I_B/r)$, where r is distance from beam to probe. Four probes, each 90° apart, were actually used at each axial location to account for geometric correction factors. The downstream $\dot{B}_\theta$ scale is 2.5 times more sensitive than the upstream.